Journal of Magnetic Resonance **143,** 69–78 (2000)
doi:10.1006/jmre.1999.1983, available online at http://www.idealibrary.com on IDEAL®

Small Volume Flow Probe for Automated Direct-Injection NMR Analysis: Design and Performance

Ronald L. Haner,* William Llanos,* and Luciano Mueller†

**Varian NMR Systems, 3120 Hansen Way, Palo Alto, California 94304; and †Bristol-Myers Squibb, Mail Stop: H23-2, P.O. Box 4000, Princeton, New Jersey 08543-4000*

Received June 10, 1999; revised November 11, 1999

A detailed characterization of an NMR flow probe for use in direct-injection sample analysis is presented. A 600-MHz, indirect detection NMR flow probe with a 120-μl active volume is evaluated in two configurations: first as a stand-alone small volume probe for the analysis of static, nonflowing solutions, and second as a component in an integrated liquids-handling system used for high-throughput NMR analysis. In the stand-alone mode, ^{1}H lineshape, sensitivity, radiofrequency (RF) homogeneity, and heat transfer characteristics are measured and compared to conventional-format NMR probes of related design. Commonly used descriptive terminology for the hardware, sample regions, and RF coils are reviewed or defined, and test procedures developed for flow probes are described. The flow probe displayed general performance that is competitive with standard probes. Key advantages of the flow probe include high molar sensitivity, ease of use in an automation setup, and superior reproducibility of magnetic field homogeneity which enables the practical implementation of 1D T2-edited analysis of protein–ligand interactions. © 2000 Academic Press

Key Words: **direct-injection NMR; SAR by NMR; high-throughput screening; LC-NMR; NMR probe.**

INTRODUCTION

Traditionally, most NMR technological innovations have focused on extracting an extensive set of information from a single sample. An increasing need appears, however, for strategies that permit the collection of a limited set of data from a large number of samples rapidly. For example, combinatorial synthesis may produce a large number of related compounds which require the rapid measurement of a limited set of NMR spectra per sample. Likewise, in NMR-based screening (SAR by NMR) one type of spectra (e.g., a ^{1}H–^{15}N HSQC spectrum) is recorded in a large set of compound mixtures. These new methods require fast, cost-effective NMR data collection and analysis and generally favor the use of relatively small sample volumes combined with some method of automated sample placement, data acquisition, and processing.

A key component of a high-throughput NMR data collection setup is the NMR probe head. In this paper we describe a novel, tubeless NMR probe which features in its core a volume-optimized, fixed geometry sample chamber (flow cell). Sample loading of the probe is achieved via a low diameter tube that is typically connected to a liquids-handling robot. Hence, in the proposed setup, NMR solutions are transferred directly into the so-called flow-injection probe from an external set of sample wells. Probes for tubeless NMR, commonly called flow probes, have not yet been characterized in detail in the literature. The purpose of this paper is to examine the feature performance of a new type of flow probe that has been optimized for data collection in the stopped-flow mode. Detailed comparisons are made to standard NMR probes, particularly pertaining to factors that are relevant to high-throughput NMR methods such as SAR by NMR (*1, 2*) screening.

Here, we compare the performance of a 120-μl active volume flow probe to standard commercial 3- and 5-mm probes of related design. The active volume (120 μl) of the flow probe represents an intermediate between the corresponding active sample volumes in 5- and 3-mm (microsample) probes, providing a set of performance markers well suited to displaying and identifying trends. However, no rigorous comparisons and statistical analyses of probe performances were carried out. The overall probe radiofrequency (RF) designs of the depicted probes are sufficiently similar to afford meaningful comparisons. Thus, the observed differences in probe performance can be attributed primarily to the variations in sample geometries.

The maximum overall sample throughput or total data collection time per sample is an important performance characteristic of an NMR probe head. The data collection time per sample in a flow probe can be written as

$$t(\text{total}) = t(\text{inject}) + t(\text{equilibrate}) + t(\text{data acquisition}) + t(\text{retrieve}) + t(\text{rinse}). \quad [1]$$

It will be shown that the equilibration times t(equilibrate) in flow and 5-mm probes are comparable. In addition, the sum total of t(inject) and t(retrieve) does not exceed by a significant amount the time needed to load tubes into a tube-holding probe by a robotic sample changer. Only the time required for rinsing the flow probe, t(rinse), prior to loading of a new sample has

1090-7807/00 $35.00

no counterpart in the NMR tube-based mode of data collection. This latter time typically represents an insignificant percentage of t(total) due to the high efficiency of the chosen sample loading protocol.

In summary, flow-based sampling methods are well-established and used within many types of general analytical instrumentation (*3*) and can be used to inject samples into NMR probes with integrated sample tubes called flow cells (*4, 5*). It will be shown in this paper that the depicted novel flow probe is highly competitive with standard tube-holding probes in achieving high-throughput data collection in large sets of samples.

DESCRIPTION OF FLOW PROBE

The flow probe design used in this study grew out of the development of a liquid chromatography (LC) NMR system (*6*). The flow probe differs from a regular NMR probe by featuring a permanently mounted sample chamber (flow cell) centered within the core of the radiofrequency detector coil. Figure 1 depicts the relative positions of NMR sample tubes and flow cell in regular 5- and 3-mm probes and in the flow probe, respectively. The solid rectangles represent the diameters and lengths of the Helmholtz-shaped proton RF coils. Both the bottom and the top ends of the flow cell are connected to 1/16“ od PTFE tubes which terminate into PEEK LC union connectors at the base of the probe. These PTFE tubes connect to the flow cell inlets by inert, adhesive-free, compression fittings.

The conical tapering of the inner diameter of the flow cell facilitates sample flow and reduced magnetic field inhomogeneity (*6–9*). The specific flow cell described here (*10*) differs in part from other designs of tapered flow cells by featuring a constant outer diameter and a length that considerably exceeds the NMR-sensitive region and by the use of quartz. When the probe is inserted in the magnet, the flow cell is aligned with the external magnetic field B_0. This design ensures that magnetic field distortions due to susceptibility differences between the aqueous buffer and the flow cell do not extend into the active region of the flow cell. The thick-walled quartz at each end of the sample chamber has the benefit of featuring a considerably closer match in bulk magnetic susceptibility to water than thin-walled Pyrex or air. Thus, the reduction of the flow cell volume to about twice the active volume within the proton detector coil still yielded acceptable proton lineshapes (see Table 2). The thick-walled stems of the flow cell can withstand the high mechanical pressures associated with compression fittings and permit the fabrication of quartz cells with exceptionally high levels of structural symmetry.

A NMR sample solution is inserted into the flow cell through the bottom inlet at a maximum flow rate that maintains laminar flow until the sample chamber is filled completely. Retrieval of the NMR sample is preferably done again through the bottom inlet. As depicted in greater detail in a subsequent section, this push–pull mode of sample change offers considerable benefits relative to a flow-through mode of operation.

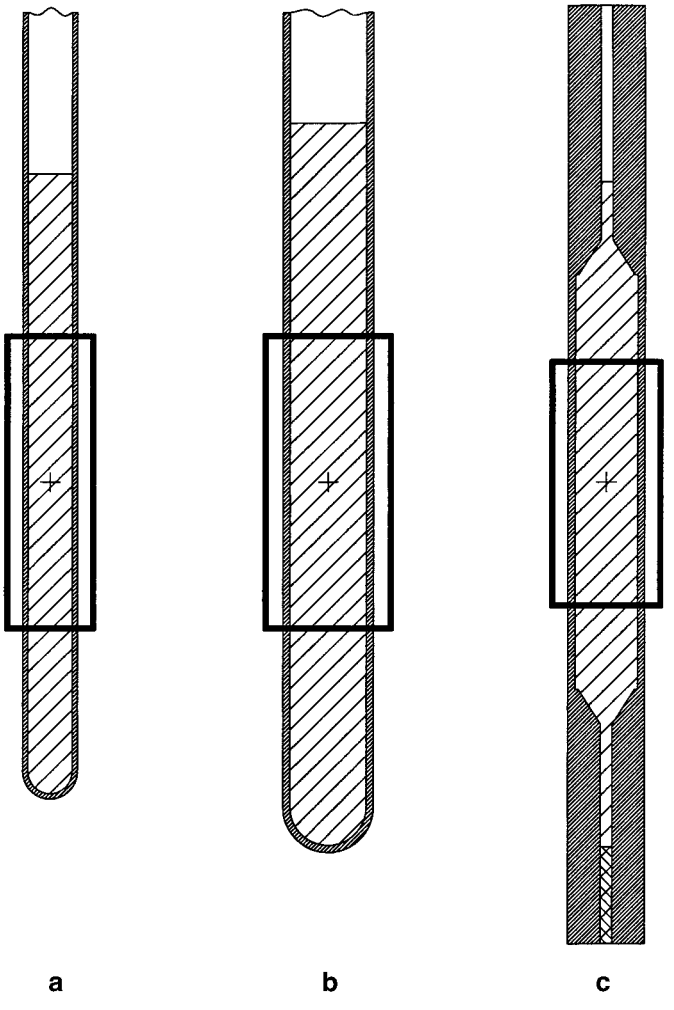

FIG. 1. Cross-sectional drawing showing the active volumes and estimated minimum sample volumes for the probes used in this study. The lengths and diameters of the RF coils are indicated by the rectangles, and the crosshatched sample regions within the rectangles represent the NMR active volumes. The full crosshatched regions within the tubes show the approximate minimum sample volumes, V_{MIN}. The double crosshatched region at the lower end of the flow cell depicts the approximate location and boundary of the optional push solvent. Diagrams show (a) the 3-mm probe, (b) the 5-mm probe, and (c) the 3.4-mm-id flow probe with 120 μl active volume.

Like regular NMR probes, flow probes can be equipped with indirect detection single and/or double resonance resonators to enable [^{1}H, ^{15}N], [^{1}H, ^{13}C], or [^{1}H, ^{15}N, ^{13}C] double or triple resonance experiments, respectively. In addition, flow probes readily accommodate actively shielded pulse field gradient coils.

The geometry of the proton detection coil in the flow probe closely resembles the prevalent geometry in regular NMR probe featuring Helmholtz saddle coils (see Fig. 2) with length L_{RF}, radius R_{RF}, and window angle Θ. For each probe used, the window angles of the proton detection coils were equivalent.

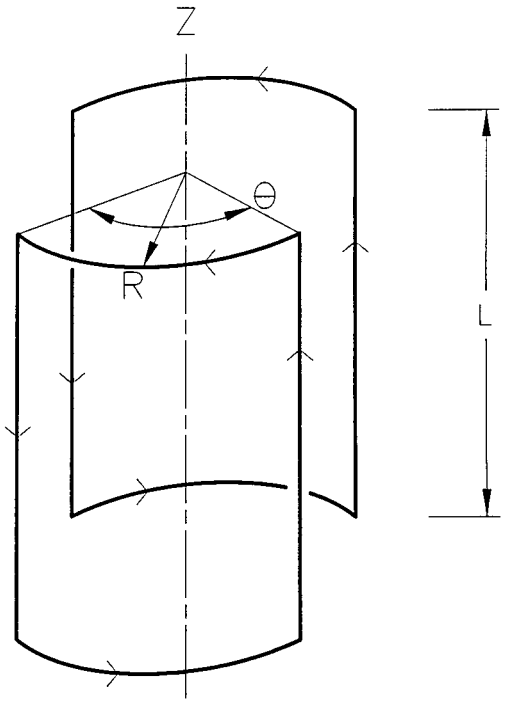

FIG. 2. Diagram showing the relevant dimensions of saddle coils for use in this paper. The dimensions shown pertain to the innermost surfaces and edges of the coil conductor. The region on the surface of the winding cylinder, with a perimeter defined by either of the two conductive loops, is called the "window."

A pair of cylindrical Faraday shields (also called RF shields), separated symmetrically above and below the coil midplane by the RF coil length, is placed at an intermediate diameter between the proton RF coil and the flow cell (*11*). These shields suppress the pickup of NMR signal from the fringes of the detector coil and thereby improve lineshape and enhance sensitivity performance in dielectrically lossy samples (aqueous solutions with high ionic strength).

Because both the flow probe and the regular sample tube NMR probes are equipped with similar geometry saddle coils, the active coil volume in either probe can be approximated by

$$V_c = 2L_{RF}\pi(R_{RF})^2, \quad [2]$$

where L_{RF} and R_{RF} represent length and radius of the detector coil (Fig. 2) and the factor 2 approximates the magnetic energy coupling to the exterior of the coil cylinder.

The active sample volume can be approximated by

$$V_s = L_{RF}\pi(R_s)^2, \quad [3]$$

where R_s represents the inside diameter of the sample tube or flow cell.

Hence, the effective coil filling factor (*12*) can be approximated by

$$\eta = V_s/V_c = (R_s)^2/[2(R_{RF})^2]. \quad [4]$$

At a given magnetic field strength and sample temperature, the probe sensitivity, or signal-to-noise ratio (S/N), is primarily affected by the respective volumes V_s, V_c, and the quality (Q) factor of the resonator circuitry as depicted in Eq. [5]:

$$S/N \propto \eta V_c^{1/2} Q^{1/2} = (V_s/V_c^{1/2})Q^{1/2}. \quad [5]$$

The filling factor η generally decreases with shrinking sample diameter, because both the wall thickness of the sample tube and flow cell and the air gap between the outer wall of the tube and the detector coil cannot be shrunk below a minimum threshold. Therefore, as shown in Table 1, the filling factor η of the flow probe is lower than in a 5-mm probe but higher than in a 3-mm microsample probe. Due to its rigid positioning the flow cell accommodates higher flow rates of temperature control air (VT-air) thereby allowing a tighter air gap between flow cell and detector coil.

PERFORMANCE OF FLOW PROBE

Essential performance characteristics of NMR probes are sensitivity, lineshape, RF field homogeneity, and time require-

TABLE 1
Comparison of Detector Coil Parameters and ^{1}H Sensitivities at 600 MHz[a]

	Standard 3 mm	Flow probe 120 μl	Standard 5 mm
Sample diameter, $2R_S$	2.4 mm	3.4 mm	4.2 mm
Coil length, L_{RF}	16 mm	13 mm	16 mm
Active volume, V_S	72 μl	120 μl	220 μl
Minimum sample volume, V_{MIN}	150 μl	270 μl	550 μl
S/N {2.00 mM sucrose in D_2O}	62	103	154
S/N {2.00 mM sucrose w. 250 mM NaCl in D_2O}	59	88	120
$(S/N)_{normalized}$ {2 mM sucrose}	0.40	0.67	1.00
$\eta V_c^{1/2} Q^{1/2}$, no salt, normalized	0.43	0.68	1.00
$(S/N)_{normalized}$ {2 mM sucrose w. 250 mM NaCl in D_2O}	0.49	0.73	1.00
$\eta V_c^{1/2} Q^{1/2}$ {w. 250 mM NaCl in D_2O, normalized}	0.50	0.76	1.00
$(S/N)/V_{MIN}$ {2 mM sucrose}	1.47	1.36	1.00
$(S/N)/V_{MIN}$ {2 mM sucrose w. 250 mM NaCl in D_2O}	1.80	1.49	1.00
S/N {0.1% ethylbenzene/ $CDCl_3$}	451	Not measured	1062

[a] Sucrose and ethylbenzene linewidths without line broadening averaged 1.5 ± 0.1 Hz in all cases. For sucrose, samples were measured without spinning and a 1.0-Hz exponential line broadening was applied prior to FT. Ethylbenzene was measured with the sample spinning, using 1.06 Hz of exponential line broadening.

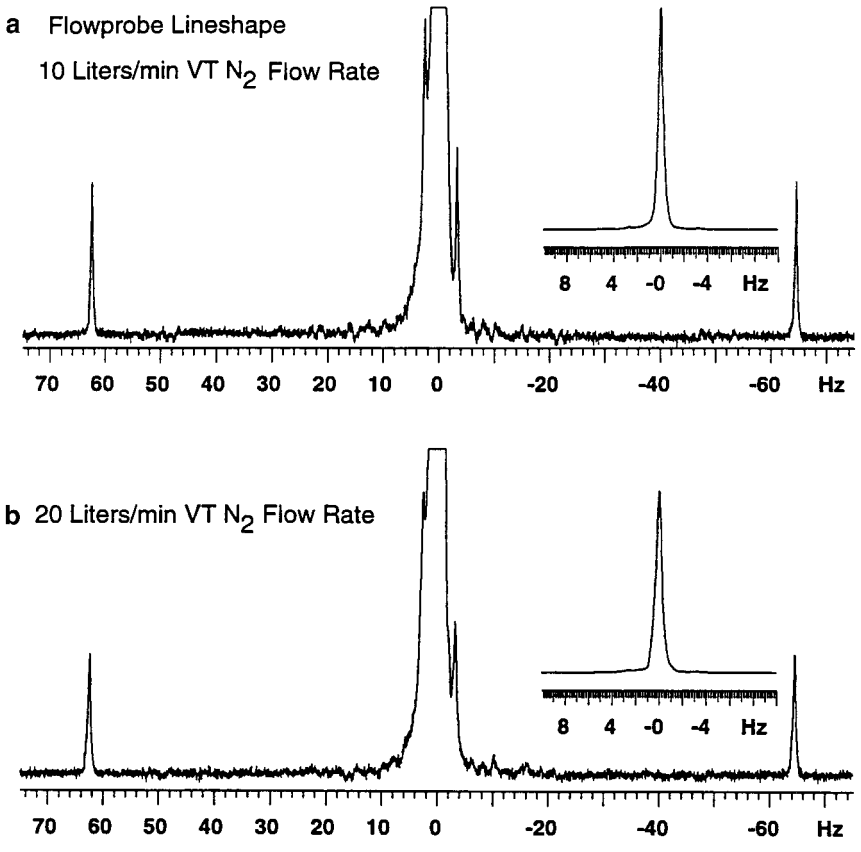

FIG. 3. Proton lineshape at 600 MHz of 50 mM sodium acetate in 99% D_2O at 30°C measured with a 120-μl active volume, 3.4-mm-id flow probe. Spectrum (a) was measured using a standard VT N_2 flow rate of 10 L/min, and spectrum (b) was measured using a VT N_2 flow rate of 20 L/min. Each spectrum shown in (a) and (b) has the same vertical scale. Insets show the shape and resolution of the upper portion of the lines and have the same vertical scale with respect to each other.

ment to achieve a homogeneous temperature across the active sample volume after the loading of the sample into the probe. Comparisons of these parameters are made using a flow probe (Varian, prototype model) and standard probes of 5-mm tube diameter (Varian, Model 00-958566-60) and 3-mm tube diameter (Varian, Model 00-958566-46). In addition, we assessed the issue of cleansing of the sample chamber prior to loading a new sample in the flow probe—a unique issue facing this type of probes. All tests were performed on Varian Inova 600-MHz NMR spectrometers.

Resolution and Lineshape

At the outset of flow probe project it was not obvious that the restricted volume flow cell would produce competitive proton NMR lineshapes. In order to avoid volatile solvents during testing, all measurements in the flow probes were conducted in aqueous solutions, although the flow probe has been demonstrated to produce quality spectra in organic solvents such as chloroform. A solution of 50 mM sodium acetate in 99.9% D_2O was chosen to perform both lineshape and temperature equilibration tests. The acetate produces a sharp singlet at half height as seen in Fig. 3. At 0.5% of the height of the methyl peak, satellite lines are visible due to one- and two-bond proton–carbon J-couplings to the methyl and carbonyl carbon, respectively. The two-bond coupling ($^2J_{CH}$ = 5.9 Hz) can be readily suppressed by band-selective carbonyl decoupling. The lineshape data in Table 2 confirm that the flow probe produces comparable lineshapes to the regular NMR probes. Shimming of the samples was performed in a straightforward manner using the automated gradient shimming algorithm followed by retouching of the low-order radial shims as well as the $z1$ gradient. However, relatively larger values of $z4$–$z6$ are

TABLE 2

^{1}H Lineshapes at 600-MHz: Full Widths Measured as Fractions of the Total Peak Height; 50 mM Sodium Acetate in 99% D_2O at 30.0°C

		50%	0.55%	0.11%
Flow probe 120 μl	Stationary	0.45 Hz	5.2 Hz	9.0 Hz
Standard 5 mm	Nonspinning	0.38	3.6	8.0
Standard 3 mm	Nonspinning	0.44	5.3	9.0

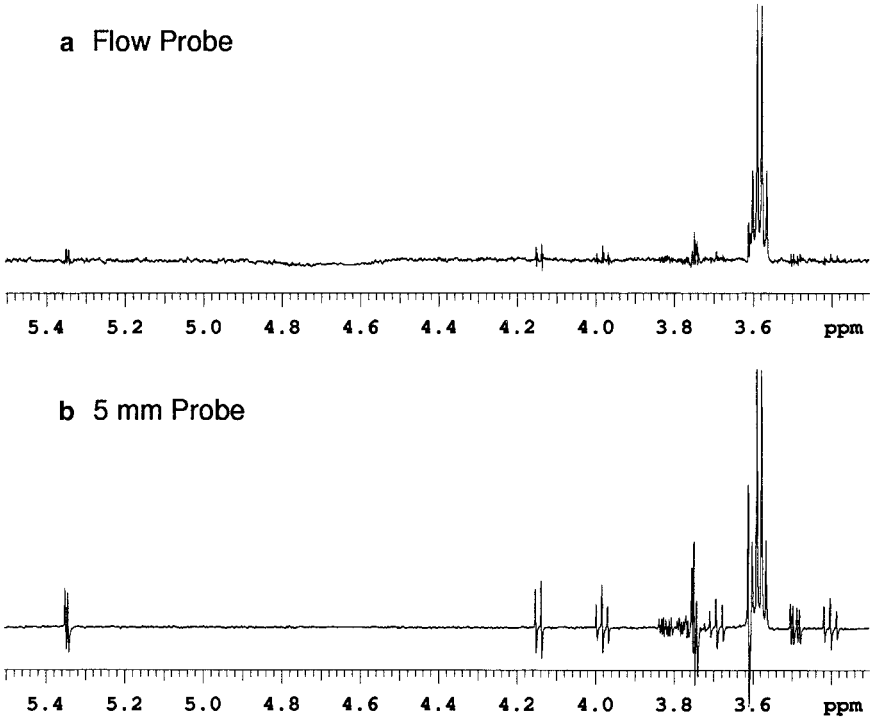

FIG. 4. Proton lineshape reproducibility test at 600 MHz showing the sucrose and sucrose–ethanol difference spectra for (a) samples injected into the 120-μl active volume, 3.4-mm-id flow probe and (b) samples (700 μl) placed into individual 5-mm tubes, using the 5-mm probe. Both spectra have 1.0 Hz of exponential broadening. The results are representative for the effort used and are not necessarily fully optimized.

needed to achieve the reported lineshapes due to the relatively short length of the large id portion of the flow cell, whose total volume is slightly less than twice its active volume.

Reproducibility of Magnetic Field Homogeneity

The flow probe features a remarkable reproducibility in lineshape and resolution as evidenced by the following subtraction test. This stability in magnetic field homogeneity and bulk susceptibility is most likely a result of the rigid geometry of the flow cell whose schematic cross section is depicted in Fig. 1. Spectra were recorded in an alternate fashion in samples of 2 mM sucrose in D_2O followed by 2 mM sucrose in D_2O doped with 2 mM ethanol (both types of samples were derived from the same stock sucrose stock solution). No push solvent was used to pump the sample into the flow probe (total transfer volume of 620 μl, one rinse cycle prior to sample loading). The 5-mm probe was loaded with samples containing 700 μl of liquid. Prior to data collection the samples were equilibrated for 3 min. No retouching of the shim gradients was performed between successive data collections. The HDO line was suppressed using WET (*13, 14*). The difference spectra, of which a representative set is depicted in Fig. 4, consistently produce superior subtraction of the sucrose lines in the flow probe. An attempt to use hand-picked, matched 5-mm sample tube holders (spinners) failed to improve the subtraction quality in the 5-mm probe. The superior reproducibility of magnetic field homogeneity in successive samples renders the flow probe most suitable for 1D-type NMR-based screening (*2*).

Sensitivity

Having established the lineshape performance, it was important to test the proton sensitivity performance of the flow probe. We were interested both in assessing sensitivity in the usual sense, relative to a given standard sample concentration, and in relative molar sensitivity given a limited amount of sample. The molar sensitivity is the sensitivity divided by the approximate minimum volume of sample (V_{MIN}) needed to achieve a suitable lineshape. The majority of proton sensitivity measurements were performed using the anomeric proton resonance in a solution of 2.00 mM sucrose in 99.9% D_2O. The temperature of the NMR samples was equilibrated at 30°C with a VT N_2 flow rate of 10 L/min. The NMR samples were shimmed to achieve a linewidth within the doublet of the anomeric resonance of less than 1.6 Hz. The HDO signal was suppressed by lower power CW presaturation during the relaxation delays. The sucrose S/N ratios represent sum averages over 10 successive single transient measurements using an acquisition time of 2 s and a relaxation delay between successive experiments of 30 s.

In addition, sealed samples of 0.1% ethylbenzene dissolved in 99.98% $CDCl_3$ were measured in the standard probes at ambient temperature. All S/N ratios were measured using a

TABLE 3
^{1}H RF Homogeneity at 600 MHz, as Intensity Ratios Relative to a 90° Pulse

	Standard 3 mm	Flow probe 120 μl	Standard 5 mm
$I(450°)/I(90°)$	91%	87%	83%
$I(810°)/I(90°)$	84%	78%	71%
Filling factor, V_S/V_C	0.13	0.17	0.19
Aspect ratio, $L_{RF}/2R_S$	6.7	3.8	3.8
$R_{RFS} - R_S$, normalized	0.8	0.5	1.0

noise band of 200 Hz. In the sucrose test, which could be performed on all three probes, the experimental signal-to-noise ratios were derived from the anomeric resonance of sucrose (2 mM sucrose in D_2O). The normalized S/N values listed in Table 1 were in close agreement with the expected theoretical values ($\eta\ V_c^{1/2}\ Q^{1/2}$) corresponding to Eq. [5] for samples with and without added salt. Due to the constricted volume of the flow cell, the flow probe allows one to concentrate a given amount of sample into a smaller volume. This translates into improved relative molar sensitivity of the flow probe and the 3-mm probe relative to the standard 5-mm probe, which requires a sample volume of 550 ml in regular NMR tubes. The use of microsample tubes (Shigemi) with susceptibility-matched plugs would boost the molar sensitivity of the 5-mm probe as well. It is important to bear in mind, however, that susceptibility-matched plugs cannot be easily inserted into NMR tubes in an automated fashion. Hence, the flow probe provides a higher molar sensitivity than a standard 5-mm probe when integrated in a robotic sample loading setup. In high ionic strength samples (high salt content), further improvements to the molar sensitivities are realized in the flow probe and the 3-mm probe in comparison to the standard 5-mm probe (see Table 1).

Homogeneity of the Radiofrequency Field

The primary factors affecting RF homogeneity are detector coil type, the filling factor η, the location of the RF shields relative to the detector coil, and the aspect ratio of the active volume $L_{RF}/2R_S$. All probes which were utilized in this study featured saddle-shape Helmholtz coils. Hence, differences in observed RF homogeneity are dominated by the filling factors and the relative placements of the RF shield. The decrease in the filling factor in the flow probe, and more significantly in the 3-mm probe, is primarily due to a greater decrease in the sample diameter relative to the detector coil diameter. This enhanced reduction in sample radius R_S confines the sample to a more homogeneous B_1 region within the detector coil and thereby causes an improvement in RF field homogeneity as documented in Table 3. The RF homogeneity data in Table 3 indicate that the proton RF homogeneity improvements relative to the 5-mm probe are greater than what one expects from the difference in the filling factor η. The observed additional enhancement in RF field homogeneity in the flow probe can most likely be attributed to a closer relative placement of the RF shields in the flow probe. This tighter geometry of RF shields and detector coil surrounding the flow cell tends to restrict and more sharply define the B_1 distribution thereby benefiting RF field homogeneity. The aspect ratio $L_{RF}/2R_S$, however, seems to have a limited impact on the proton RF field homogeneity in these probes.

The ^{15}N RF homogeneity was measured as a nonroutine test using a sample of 2% ^{15}N-enriched benzamide in dry d_6-DMSO with 0.2% $Cr(acac)_3$. A ^{1}H–^{15}N heteronuclear echo sequence was used, and the ^{15}N RF homogeneity was measured as intensity ratios of the amide ^{1}H signal relative to the ^{1}H signal resulting from a 0° ^{15}N pulse, obtained by arraying the ^{15}N pulse width. The ^{15}N transmitter was placed on resonance, the samples were not spun, and four transients were averaged per spectrum.

The ^{15}N RF homogeneity for the 120-μl flow probe was similar to the 3-mm probe, having an intensity ratio obtained with spectra using a 720° ^{15}N pulse, relative to that measured using a 0° ^{15}N pulse, of 75%. The 5-mm probe had a value of $I(720°)/I(0°)$ of 63%. The error is estimated to be $\pm$2%.

Sample Temperature Equilibration

The time requirement for establishing the desired temperature across the entire NMR sample represents an important factor affecting the quality of modern NMR probes. A short sample equilibration time translates into enhanced sample throughput. Reaching a stable homogeneous sample temperature prior to data collection is of particular importance in aqueous samples, where the magnetic field is typically locked to the temperature-sensitive D_2O-resonance. Temperature equilibration was monitored using a sample of 50 mM sodium acetate in D_2O. The methyl proton resonance of the acetate ion is sensitive to the sample temperature when the magnetic field is locked to the deuterium resonance of the aqueous solvent. The temperature equilibration curves in Fig. 5 indicate that both the flow probe and the 5-mm probe reach the set equilibrium temperature at a comparable rate when comparable VT-air flows were employed (~10 L/min). Due to its greater surface to volume ratio, the 3-mm probe equilibrates at a considerably faster rate as expected. The relatively better surface to volume ratio of the flow probe compared to the 5-mm probe does not translate into a more rapid temperature equilibration. This can be explained by the narrower air gap between flow cell and proton detector coil, which slightly hampers VT-air flow as outlined in the previous section on probe sensitivity. Fortunately, the rigid geometry of the flow cell accepts an increased VT-air flow rate of up to 20 L/min without producing any deterioration in proton NMR lineshape and without introducing vibrational artifacts. At a VT-air flow rate of 20 L/min the equilibration curve of the flow probe ap-

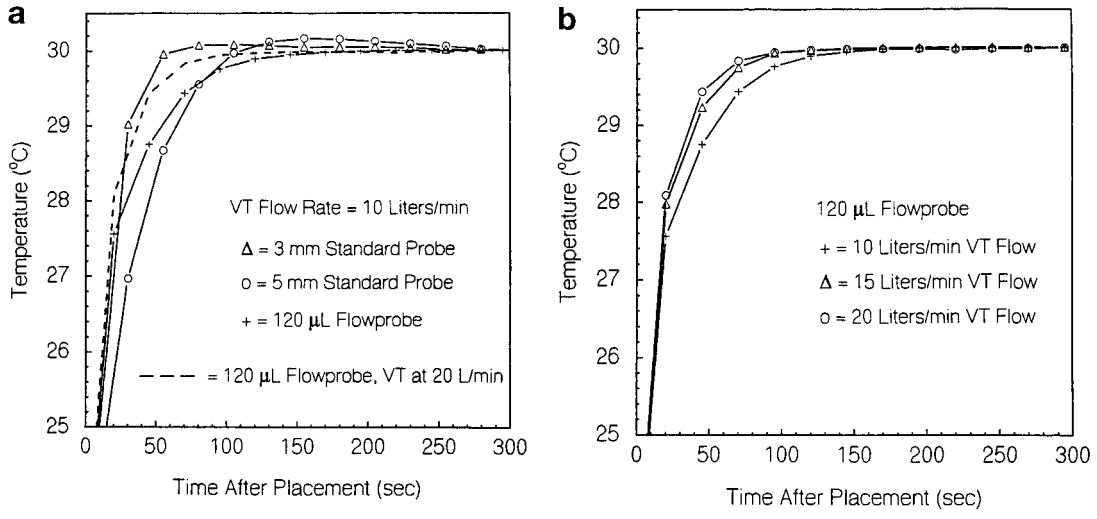

FIG. 5. Plot (a) shows the rate of thermal equilibration of newly placed aqueous samples for the 120-μl active volume, 3.4-mm-id flow probe (+), the 3-mm probe (△), and the 5-mm probe (○), using VT N_2 flow rates of 10 L/min. The dashed line indicates the flow probe sample equilibration using a VT N_2 flow rate of 20 L/min. The time scale for each probe was defined as zero at the moment that the sample enters the active volume. Plot (b) shows the rate of thermal equilibration of newly placed aqueous samples for the 120-μl active volume flow probe at VT N_2 flow rates of 10 (+), 15 (△), and 20 (○) L/min.

proaches the excellent equilibration curve of the 3-mm probe shown in Fig. 5.

Carryover between Successive Samples in the Flow Probe

The utility of the flow probe critically depends on the ability to clean out the sample chamber prior to loading a successive sample. The need for excessive, time consuming rinsing of the sample chamber would neutralize the relative superior molar sensitivity of the flow probe (see Table 1). Early on it was discovered that the need for extensive rinsing between samples is greatly reduced when both loading and removal of sample is performed through the bottom of the flow cell compared to a flow-through LC-type sample retrieval through the outlet at the top of the flow cell. The insertion and ejection of the sample through the bottom inlet of the flow cell has two key benefits. First, the creation of air bubbles in the sample chamber, whose presence would seriously deteriorate magnetic field homogeneity, is greatly diminished. In fact, the excellent reproducibility of magnetic field homogeneity in the flow probe as depicted in a previous section can be attributed to a lack of air bubble formation. Second, removal of the sample though the bottom of the flow cell, assisted by introducing compressed nitrogen through the top inlet, physically removes most of the sample before the rinse solvent is pushed into the probe.

The rinse test was performed using a sample of 3 mM chicken egg white lysozyme (Sigma) in 99.9% D_2O. Using a Gilson liquid handler Model 215, a sample of 250 μl of lysozyme was injected into the flow probe followed by a push volume of 350 μl plain D_2O. Prior to data acquisition, the sample was equilibrated for 5 min. The WET scheme was used to suppress the HDO signal. Figure 6 summarizes the results of the rinse test. After one rinse cycle the integrated intensity over the spectral region between 4.6 and −1 ppm indicates that one rinse cycle using plain D_2O reduces the concentration of protein 100-fold. After two rinse cycles signal from residual lysozyme dropped to the edge of detection ability. Each rinse cycle consumes a time slot of about 100 s. Each emptying of the sample chamber reduces the amount of residual sample in the flow cell by at least 10-fold. Hence, removal of the protein sample reduces the level of lysozyme in the flow cell at least 10-fold. Removal of the first load causes another 10-fold reduction in protein giving rise to the observed 100-fold reduction of sample at the end of the first rinse cycle. Removal of the second batch of rinse solvent gives rise to another 10-fold reduction in protein concentration resulting in a 1000-fold reduction of protein at the end of the second rinse cycle. In summary, two rinse cycles should provide adequate separation between adjacent samples in the overwhelming number of cases. In experiments where ligand-binding to a target protein is assessed one rinse cycles may already suffice.

Sample Recovery

The flow probe setup permits an almost full recovery of the sample. For concentrated protein solutions, a single cycle recovery is approximately 90% based on the rinse experiment shown in Fig. 6. For smaller molecules with less affinity to the inner surfaces, the single cycle recovery is approximately 95%. If needed, it is possible to improve this percentage by experimentation and optimization of conditions. A second retrieval cycle can be implemented by keeping the aliquot of diluted rinse fluid.

Some drop in sample concentration may occur when plain solvent is used as the push volume. Pushing a minimum active sample volume of about 250 μl into the probe by plain solvent

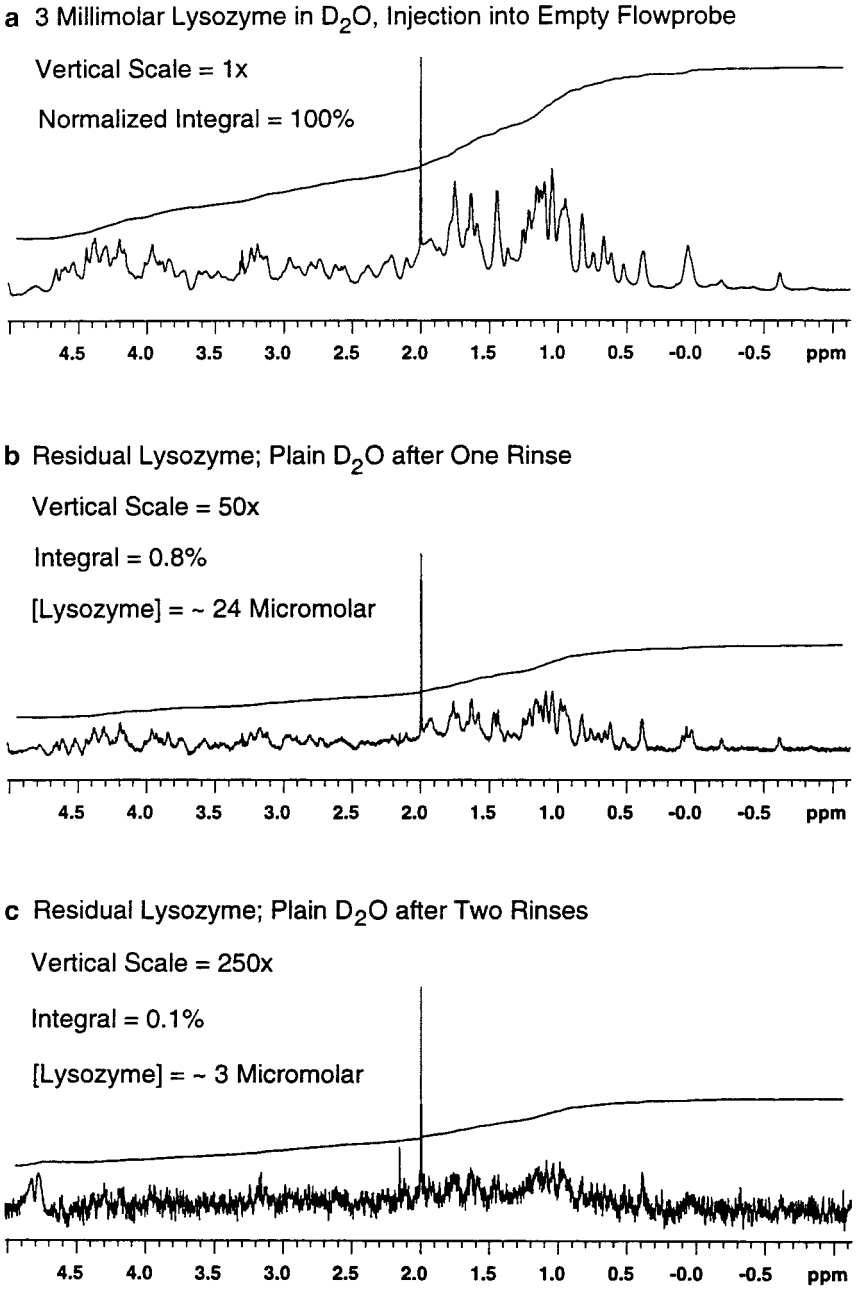

FIG. 6. Rinse efficiency as measured by lysozyme carryover. Spectrum (a) is a 600-MHz ^{1}H measurement of 3 mM lysozyme in 99% D_2O using 64 transients. Spectrum (b) is a ^{1}H measurement of plain D_2O, showing the residual lysozyme after one rinse cycle with plain D_2O (effectively two dilution cycles) using the same spectrometer conditions and plotted with a vertical expansion of 50× relative to (a). Spectrum (c) is a ^{1}H measurement of plain D_2O showing the residual lysozyme after two plain D_2O rinse cycles (effectively three dilution cycles) using the same spectrometer conditions and plotted with a vertical expansion of 250× relative to (a). Spectra (b) and (c) were compared to (a) using integrals, and residual concentrations were estimated to be 0.024 and 0.003 mM respectively, assuming uniform mixing after injection of plain D_2O. For smaller aqueous molecules having less affinity to the inner surfaces, rinse effectiveness is greater.

helps to conserve the sample, but some dilution cannot be prevented at the push solvent/NMR sample interface, although such mixing does not affect the sample concentration in the active volume during the course of typical NMR experiments, such as proton 1D or $^{1}H–^{15}N$ HSQC.

Automation of Sample Loading

The flow probe can be readily interfaced with a liquids-handling robot such as a Gilson liquid handler Model 215. This type of liquids handler accepts 96-well blocks or 384 microtiter

plates, which are commonly used in high-throughput screening assays. Hence, the flow probe allows one to readily interface an NMR spectrometer with standard high-throughput screening hardware, thereby using the spectrometer as a specialized detector of intermolecular interactions. One potential drawback of using a flow probe interfaced to a robot is the insertion of additional inactive (dead) volume in the liquids mixing chamber of the liquids handler and the tubing which links the flow cell to the mixing chamber of the liquids-handling robot. If one uses tubing with an inside diameter of 0.010 in., the dead volume amounts to about 150 μl. However, this dead volume can be readily filled with plain H_2O or D_2O depending on the type of sample that is used by pushing a sample that slightly exceeds the flow cell with plain solvent into the flow cell. During the course of a typical NMR experiment negligible amounts of plain solvent diffuse into the active region of the flow cell. For this reason, the minimum sample volume that is needed to perform an experiment in the flow probe is only 270 μl. This dead volume includes about 40 μl of nonaspired sample at the bottom of the 96-well blocks which are mounted on the liquids handler. The flow rate of 0.3 ml/min allows reliable loading of aqueous samples and is a conservative, nonoptimized rate for aqueous samples. Lower viscosity solvents such as acetonitrile of chloroform permit more rapid rates of sample transfers to and from the flow probe. The liquids handler and the flow of data acquisition using the flow probe are controlled by the VAST software package.

DISCUSSION

The depicted novel flow probe features an active volume that is intermediate in size between a standard 5-mm and a standard 3-mm probe. As in the standard probes, the flow probe features saddle-type RF coils and a cylindrical sample chamber. Thus, the primary unique characteristics of the flow probe stem from the choice of a static sample chamber whose relative size and geometry impact sensitivity, lineshape, and other key characteristics.

Resolution, lineshape, and ease of shimming in the flow probe resemble that of the standard 5- and 3-mm probes, although the flow probe features a minimum sample volume that is comparatively small for its sample diameter. Furthermore, we found the lineshapes to be highly reproducible in the flow probe. This excellent reproducibility in lineshape, which is expected to facilitate 1D SAR by NMR experiments (*2*), can be attributed primarily to two factors. First, the fixed geometry of the sample chamber greatly reduces variations in bulk magnetic susceptibility between samples. Second, the occurrence of air bubbles in the sample chamber of the flow probe is virtually nonexistent. This lack of air bubbles is aided by the fact that NMR samples are both loaded and removed from the bottom port of the sample chamber. Furthermore, the conical shape of the ends in the sample chamber reduces turbulence in sample flow. The end effects in magnetic susceptibility of the relatively small sample chamber, approximating twice the active volume, are reduced by the choice of thick-walled quartz at each end of the sample chamber assembly. The use of glass, which is susceptibility matched to water, would permit an additional reduction in the size of the sample chamber. In addition, the closer RF shields in the flow probe tend to confine the active sample volume more tightly and thereby improve lineshape performance.

CONCLUSION

We have compared a set of NMR probes of similar layout and circuitry at the same field strength, thereby distilling probe performance characteristics in terms of sample volume and geometry. The depicted tubeless flow probe has been shown to represent a viable alternative to standard NMR probes. While achieving comparable magnetic field homogeneity as in the standard NMR probes, the flow probe offers improved sensitivity where NMR samples are limited. This is especially valuable in situations such as primary 1D or 2D SAR by NMR screening measurements (*1, 2*). The excellent reproducibility of the magnetic field homogeneity in the fixed flow cell of the flow probe facilitates the collection of clean difference spectra such as 1D NOE difference- or T_2-weighted ^{1}H 1D difference spectra (*2*).

A tubeless NMR flow probe allows for direct injection of samples from well-plates and facilitates high-throughput analysis of samples, while the depicted sample loading protocol greatly reduces leakage between adjacent samples. The opportunity to use alternative sample containers such as well-plates—a significant departure from conventional sample tubes—permits the interface and development of automation technologies common to other analytical methods. Together with calculable and reliable probe performance, direct-injection NMR provides opportunities for reduction of costs, particularly those associated with sample preparation. With the direct-injection format, the individual terms in Eq. [1] can be optimized separately for specific applications. Thus, Eq. [1] can be viewed term-by-term with greater perspectives for the development of efficient NMR sample management strategies.

ACKNOWLEDGMENTS

The authors gratefully acknowledge Thomas Barbara, Howard Hill, and Knut Mehr for reviewing the manuscript. We also thank Giang Le, Ruby Gualberto, Nancy Winward, Viresh Patel, and Bao Nguyen for their expert technical efforts.

REFERENCES

1. S. B. Shuker, P. J. Hajduk, R. P. Meadows, and S. W. Fesik, Discovering high-affinity ligands for proteins: SAR by NMR, *Science* **274,** 1531–1534 (1996).
2. P. J. Hajduk, E. T. Olejniczak, and S. W. Fesik, One-dimensional

relaxation- and diffusion-edited NMR methods for screening compounds that bind to macromolecules, *J. Am. Chem. Soc.* **119,** 12257–12261 (1997).

3. J. Ruzicka and E. H. Hansen, Flow injection analyses, part I. A new concept of fast continuous flow analysis, *Anal. Chim. Acta* **78,** 145–157 (1975).
4. P. A. Keifer, High-resolution NMR techniques for solid-phase synthesis and combinatorial chemistry, *Drug Discovery Today* **2,** 468–478 (1997).
5. P. A. Keifer, New methods for obtaining high-resolution NMR spectra of solid-phase synthesis resins, natural products, and solution-state combinatorial chemistry libraries, *Drugs Fut.* **23,** 301–317 (1998).
6. H. Barjat, G. A. Morris, M. J. Newman, and A. G. Swanson, Adaptation of commercial 500 MHz probes for LCNMR, *J. Magn. Reson. A* **119,** 115–119 (1996).
7. J. F. Haw, T. E. Glass, and H. C. Dorn, Continuous flow high field nuclear magnetic resonance detector for liquid chromatographic analysis of fuel samples, *Anal. Chem.* **53,** 2327–2332 (1981).
8. E. Bayer, K. Albert, M. Nieder, E. Grom, G. Wolff, and M. Rindlisbacher, On-Line coupling of liquid chromatography and high-field nuclear magnetic resonance spectrometry, *Anal. Chem.* **54,** 1747–1750 (1982).
9. K. Albert, M. Kunst, E. Bayer, M. Spraul, and W. Bermel, Reversed-phase high-performance liquid chromatography-nuclear magnetic resonance on-line coupling with solvent non-excitation, *J. Chromatogr.* **463,** 355–363 (1989).
10. R. L. Haner, "Flow Tube for NMR Probe," U.S. Patent 5,867,026 (1999).
11. H. D. W. Hill and M. D. Cummings, "NMR Probe Incorporating RF Shielding of Sample," U.S. Patent 5,192,911 (1993).
12. H. D. W. Hill and R. E. Richards, Limits of measurement in magnetic resonance, *J. Phys. E. 2* **1,** 977–983 (1968).
13. R. J. Ogg, P. B. Kinglsey, and J. S. Taylor, WET, a T_1- and B_1-insensitive water suppression method for *in vivo* localized 1H NMR spectroscopy, *J. Magn. Reson. B* **104,** 1–10 (1994).
14. S. H. Smallcombe, S. L. Patt, and P. A. Keifer, WET solvent suppression and its applications to LC NMR and high-resolution NMR spectroscopy, *J. Magn. Reson. A* **117,** 295–303 (1995).